Interfacial Phenomena and Heat Transfer, 1 (3): 195–205 (2013)

CONTROLLING THE MORPHOLOGY OF RING-LIKE DEPOSITS BY VARYING THE PINNING TIME OF DRIVEN RECEDING CONTACT LINES

Carmen L. Moraila-Martínez, Miguel A. Cabrerizo-Vílchez, & Miguel A. Rodríguez-Valverde*

Biocolloid and Fluid Physics Group, Applied Physics Department, Faculty of Sciences, University of Granada, E-18071 Granada, Spain

*Address all correspondence to Miguel A. Rodríguez-Valverde, E-mail: marodri@ugr.es

The variety of morphologies observed in the particle deposits produced by solvent evaporation may be ruled to a large extent by contact line dynamics and in particular, by self-pinning events described by the contact line. If the number of particles in the suspension bulk increases, more particles should be transported toward the contact line during evaporation. Increasing times of contact line pinning should lead to the same effect than particle concentration. In this work, we investigated the different ring-like deposits obtained at driven receding contact lines by varying separately nanoparticle concentration and pinning time. We used a recent methodology based on "shrinking" sessile drops to mimic the contact line dynamics of freely evaporating drops. Unlike drying drops, with this methodology the particle concentration in the drop bulk is assumed to remain mostly constant during the entire process. We concluded that no nanoparticle deposit is formed if the pinning time is reduced below a critical value for a given substrate-particle system. However, an increase of pinning time enables the ring formation even at low particle concentrations.

KEY WORDS: *ringlike deposits, driven contact lines, pinning time*

1. INTRODUCTION

Controlled drying of colloidal particle suspensions is intended to produce solute deposits on solid substrates. Diversity in the morphology of these deposits is due to the complex mechanisms behind the transport of the particles toward the substrate during solvent evaporation. The formation of ring-like deposits at the periphery of drying sessile drops containing particles is known as the "coffee stain" or "coffee ring" effect (Deegan et al., 1997). Different patterns of dried drops can be found if the liquid evaporation rate is varied in different ways such as altering the relative humidity, temperature, or pressure (Askounis et al., 2012), using a vapor atmosphere of different liquids (Majumder et al., 2012), by modifying substrate properties (Lopes and Bonaccurso, 2013). The transition from ringlike to uniform deposits is also influenced by particle properties: shape (Yunker et al., 2011), surface roughness (Lee et al., 2013; Li et al., 2013), and electric charge (Carle and Brutin, 2013). Bhardwaj et al. (2010) reported that the pH of the solution modifies the final deposit pattern. They explained the transition between different patterns by considering how the electrostatic and van der Waals forces alter the particle deposition process. In a recent work (Moraila-Martínez et al., 2013), we found that the morphology of nanoparticle deposits was modulated to a different extent by the following parameters: the strength of the particle-particle electrostatic repulsion and the substrate receding contact angle.

In an evaporating sessile drop of pure liquid, the contact angle decreases up to the receding contact angle of the substrate and then the contact line begins to recede. This time period is referred to as "pinning time" and, at fixed temperature and humidity, it depends on the drop volume, the initial contact angle, and the substrate receding contact angle. This way, different pinning time values are usually observed as the substrate used. Instead, drying sessile drops of suspended particles usually undergo "self-pinning" (Deegan et al., 1997) due to the accumulation of particles near the triple line driven by the outward capillary flow produced by the drop evaporation.

2152–5080/13/$35.00

As the particle number increases in bulk, more particles are driven toward the contact line and self-pinning is enhanced. In addition, smaller particles provide a greater number concentration (at the same volume fraction), have a greater mobility, and accumulate closer to the contact line rather than larger particles (Perelaer et al., 2008). As happens with drops of pure liquid, the range of observable contact angles on the substrate (contact angle hysteresis) can also dictate the motion of receding contact lines (Moraila-Martínez et al., 2012). This way, contact line dynamics of evaporating drops containing particle suspensions can become very complex, because local or global cycles of pinning-depinning or even perpetual pinning are observed. Shen et al. (2010) reported that a minimum time is required for the formation of ringlike deposits. They proved that when a fast evaporation of liquid is induced, the particles do not have enough time to accumulate at the contact line while it remains pinned even if there are an adequate number of particles. From the work of Bodiguel et al. (2009), it is plausible to think that the control of pinning events (duration and number) will dictate the final morphology of the ringlike deposits.

In a previous work (Moraila-Martínez et al., 2013) we found that the pinning effect of the contact line can be enhanced when the electrostatic interactions are weak. In the present work, the electrostatic interactions (substrate-particle and particle-particle) were minimized and the substrate receding contact angle was fixed. Using a methodology based on driven receding contact lines of drops (Moraila-Martínez et al., 2013), the pinning time was varied in a controlled way for a substrate-particle system and at fixed particle volume fraction.

2. MATERIALS AND METHODS

We employed polymethylmethacrylate (PMMA, 2 mm-thick sheets, CQ grade, Goodfellow) as the substrate for the deposit formation. This material was utilized due to its stable response in contact angle. The PMMA sheets were cut by laser as disks with 1.5 cm in diameter. A hole of 1 mm diameter was drilled to each sample. Before each experiment, the PMMA surfaces were cleaned ultrasonically in a detergent solution for 10 min, followed by ultrasonic rinsing in Milli-Q water. The roughness of the substrates was measured with a white light confocal microscope (PLμ, Sensofar Tech S.L.) and with an atomic force microscope (multimode scanning probe microscope, Nanoscope IV, Veeco). The details of the experimental setup used for contact angle measurements are described elsewhere (Moraila-Martínez et al., 2012). Drop profiles were analyzed with the Axisymmetric drop shape analysis-profile (ADSA-P) technique. With this approach, all the drop parameters such as contact angle, contact radius, area, volume, and surface tension were extracted.

We used commercial aqueous suspensions of spherical nanoparticles. We purchased PMMA particles (120 ± 8 nm of diameter) at volume fraction of $\Phi_V = 5\%$ to Microparticles. We also used suspensions of silica particles concentrated above $\Phi_V \geq 17.5\%$ with diameters of 22 ± 1 nm (20 nm SiO_2) and 90 ± 10 nm (90 nm SiO_2), kindly supplied by Klebosol. Although the PMMA and silica particles were negatively charged as they were delivered (at uncontrolled pH), we minimized the particle electrical charge through the medium pH using buffer solutions of low ionic strength ($\leq$0.1 mM). A sample of 10 ml of particle suspension was dialyzed against 1 L of buffer solution for 5 h and next, the buffer solution was exchanged two times. We used a dialysis tubing cellulose membrane (D9652, Sigma Aldrich) with a pore size in the range of 1–2 nm. We found from electrophoretic mobility measurements (Moraila-Martínez et al., 2013) that the minimal electrostatic interactions were reproduced at pH 2. At this pH, the PMMA particles presented colloidal stability at long times due to their non-negliglible electrostatic repulsion. Instead, we obtained the isoelectrical point of silica particles at pH 2, but it has been found that suspensions of colloidal silica are completely stable at low pH due to additional non-DLVO (Derjaguin-Landau-Verwey-Overbeek) repulsive forces (hydration forces) (Kobayashi et al., 2005).

Recently, we have developed a methodology (Moraila-Martínez et al., 2012) where the contact line dynamics of evaporating drops can be mimicked at shorter times using a nonlinear suction from the drop bulk. With this methodology, referred to as controlled shrinking sessile drop (CSSD), we are able to decouple the evaporation from the motion of triple line and to explore separately certain effects on the drying drops containing nanoparticles, as Bodiguel et al. (2009) reported using a device inspired in the dip-coating technique. The CSSD method standardizes the internal flow within shrinking drops because the flux distribution imposed, including the flow due to the sustained evaporation at the triple line, is reproducible from one experiment to another performed at fixed temperature and relative humidity. After a CSSD experiment, using large drops, no significant macroscopic evaporation was observed, even

with the slowest process. The experimental drop volume agreed with the theoretical drop volume within our experimental resolution (± 2 μL). The driven receding motion of the contact line overlaps the unnoticeable motion of the contact line due to evaporation. However, such as happens in the "coffee stain effect," the main mechanism for the accumulation of nanoparticles near the triple line using the CSSD methodology is the unmeasurable local evaporation at the wetting line. Unlike free evaporation of sessile drops, particle concentration in bulk is assumed to remain constant for a CSSD experiment. We operated in the quasistatic regime of contact line motion where the viscous effects are excluded (low capillary numbers, Ca $\ll 10^{-4}$). In this regime, the observed contact angle should be speed independent.

The total length of a standard CSSD experiment may be divided into two periods (Fig. 1): pinning time (t_p) and receding time (t_r) of the contact line. We refer to the pinning stage as the stage where the drop reveals a minimum displacement of contact line with a maximum variation in contact angle. For each stage, the same quantity of liquid is suctioned. The pinning stage in the CSSD technique occurs when the initial contact angle is decreased from a stable contact angle (usually close to the advancing contact angle) to the substrate receding contact angle. For the same volume range, we are able to increase or decrease the pinning time by changing the liquid withdrawal flow rate accordingly. The receding stage should correspond to the contact line motion of pure water. In this stage, the contact angle remained constant. It should be noticed that, with drops containing particles, when self-pinning is significant the actual length of the first pinning event will be greater than the pinning time imposed by the CSSD technique. Initially, one 220 μL drop is injected through the hole of the PMMA substrate. Since we intended to change the length of the pinning stage, two different syringes (100 μL and 250 μL) were used with two microinjectors (PSD3, Hamilton) connected to the same PC. This way, the pinning stage could be reproduced over a wider range of flow rates (100 μL syringe) and thus, with different times. Next, it was connected to the subsequent receding stage (250 μL syringe). It is worth mentioning that each suction process was performed following a nonlinear function in time to mimic the contact line dynamics of freely evaporating drops (Moraila-Martínez et al., 2013).

For PMMA substrates, when the volume of a stable water drop is reduced from 220 to 120 μL, the receding contact angle is reached with a very small displacement of contact line ($\leq 0.2 r_{\max}$). Next, when the drop volume is decreased from 120 to 20 μL, the drop recedes significantly. The different pinning times reproduced in this study are shown in Table 1. The experiments were performed in still air at room temperature (25°C) and relative humidity of 50–53%.

Contact line dynamics of a Milli-Q water drop during a CSSD experiment is shown in Fig. 2. The entire CSSD process can be divided into five well defined substages: the three first substages correspond to the pinning stage and

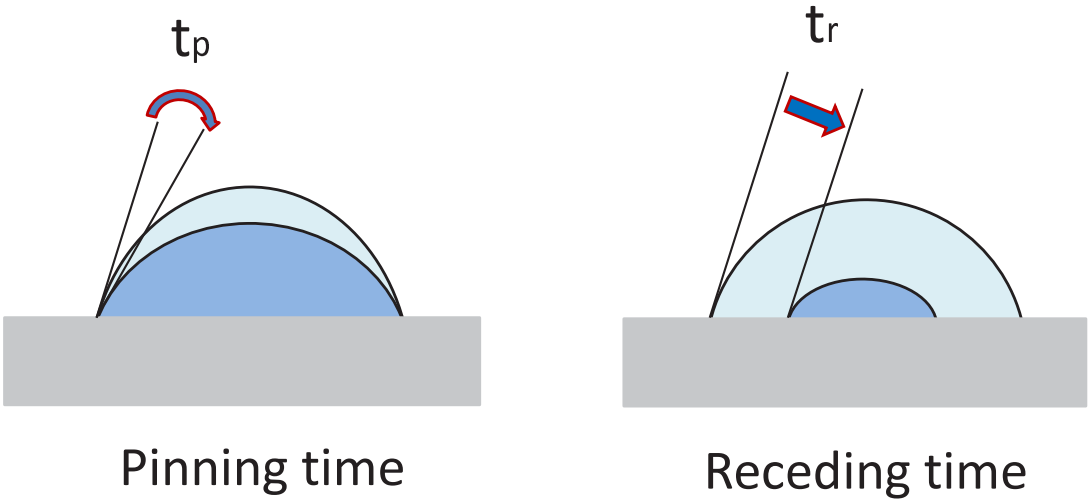

FIG. 1: Sketch of the pinning and receding stages during a controlled shrinking sessile drop (CSSD) experiment. The pinning and receding times are shown.

TABLE 1: Processes with different pinning times of contact line using the Controlled Shrinking Sessile Drop methodology

Process	Pinning time (s)	Receding time (s)	Total time (s)
PT-1	140	483	623
PT-2	273	483	756
PT-3	327	483	810
PT-4	461	483	944

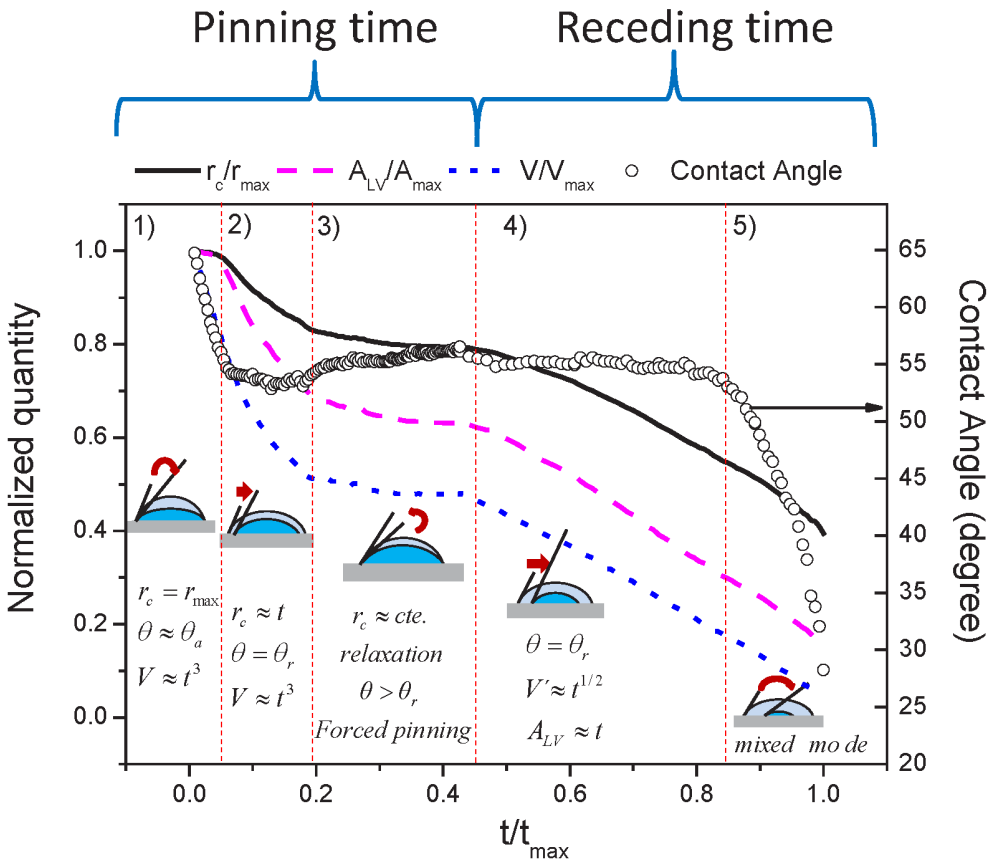

FIG. 2: Contact line dynamics of a Milli-Q water drop during a CSSD experiment. Inset numbers illustrate the five substages.

the last two to the receding stage. During the pinning stage, the drop volume follows a cubic law ($V \approx t^3$) (Moraila-Martínez et al., 2012) and during the receding stage, the drop volume decreases as the law $V \approx t^{3/2}$. In the substage 1, the total pinning of the contact line is observed while the contact angle significantly decreases from the initial value, usually close to the advancing contact angle. In substage 2, the receding contact angle is reached and consequently a small displacement of contact line is observed. The distance covered by the contact line during this displacement, in the best of the cases, was $\leq 0.2 r_{\max}$. Hence, in this work, we considered that the contact line was fairly receding when its displacement was sustained ($>0.2 r_{\max}$). During the small movement of contact line described in substage 2, the contact radius is a linear function of time ($r_c \approx t$) and the contact angle remains constant. In substage 3, an effective "pinning" of the contact line is reproduced because the contact radius decreases very slowly while the contact angle

relaxes toward a greater value. Substage 4 corresponds to a linearly decreasing liquid-vapor area ($A_{LV} \approx t$) with a constant receding contact angle, as observed in the last stages of a freely evaporating drop (Erbil, 2012). The last substage 5 reveals a mixed mode where both contact radius and contact angle decrease with time.

To explore the impact of the variation of pinning time on contact line dynamics, we performed with Milli-Q water the processes described in Table 1. For this study, the plot of contact angle as a function of the three-phase contact radius becomes helpful. This way, the quality of the surface (asperities, chemical patches) can be observed indirectly through the measured contact angles. Figure 3 confirms that the contact line dynamics of pure water was not affected by the variation of pinning time. A unique pinning event is clearly identified at $r_c/r_{\max} \approx 1$, i.e., the natural pinning of the contact line due to the substrate contact angle hysteresis.

3. RESULTS AND DISCUSSION

3.1 Nanoparticle Concentration

To examine exclusively the effect of nanoparticle concentration on the morphology of deposits, we carried out the reference CSSD experiment ($t_p = 140$ s) with 20 nm SiO_2 suspensions at pH 2 on PMMA substrates. The volume fraction was varied from $\Phi_V = 0.1$ to 10%. The different behavior of the contact line is shown in Fig. 4. At $\Phi_V = 0.1\%$ the contact line behaved such as for pure liquids. From $\Phi_V = 1$ to 5%, a stick-slip motion was detected. For $\Phi_V = 7$ and 10% the contact line remained pinned during the entire process. The arrow in Fig. 4 shows that as the concentration increased, the contact line dynamics described from a free receding motion to a perpetual pinning. This validates the role of nanoparticle concentration on the final pinning time of the contact line.

To analyze the morphology of the deposits obtained, we used a white light confocal microscope (PLμ, Sensofar Tech S.L. 50X objective). This way, the morphology information was extracted from radial profiles of each ringlike deposit. Each deposit profile was characterized by the width (covewred substrate area) and the height. The results are shown in Fig. 5. At $\Phi_V = 0.1\%$, no particle deposit was observed except for the residual spot found at the center

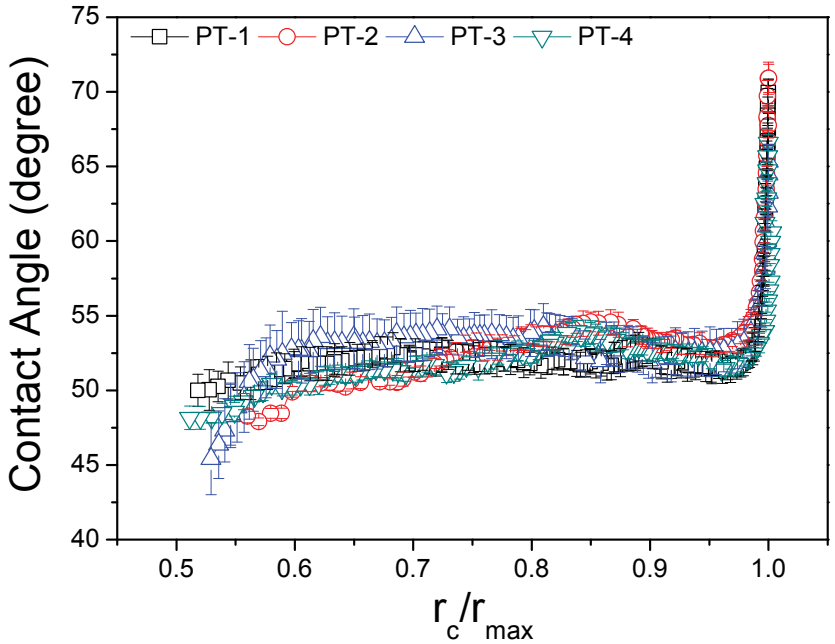

FIG. 3: Contact line dynamics of Milli-Q water on PMMA substrates during CSSD experiments performed with increasing pinning times. The contact radius was normalized by the maximum contact radius obtained in each case ($r_{\max} \approx 6$ mm). The symbols and legends correspond to each pinning time listed in Table 1.

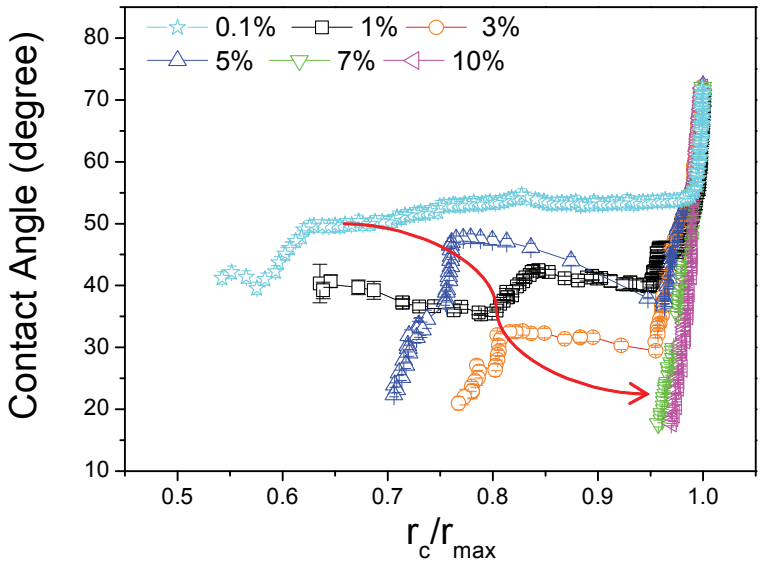

FIG. 4: Contact line dynamics of 20 nm SiO_2 suspensions at pH 2 on PMMA substrates using the CSSD technique. The concentration value was varied from $\Phi_V = 0.1\%$ to 10%. The arrow indicates the transition from a free receding motion to a total pinning of contact line.

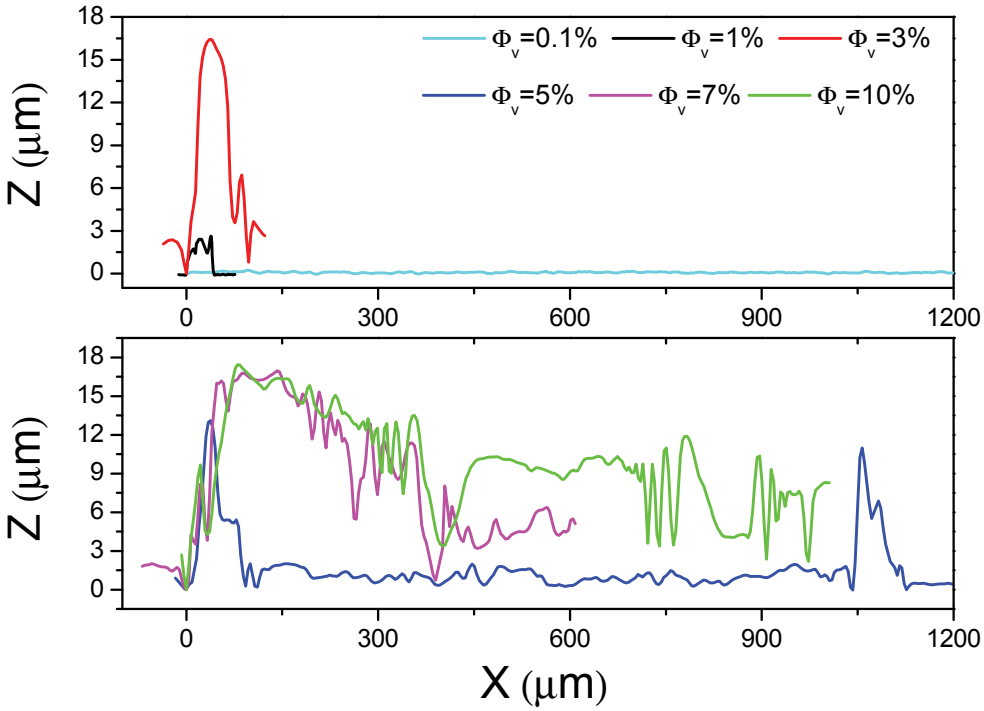

FIG. 5: Radial profiles of the ringlike deposits formed with 20 nm SiO_2 suspensions at pH 2 and different nanoparticle concentrations on PMMA substrates. At $\Phi_V = 5\%$, two concentric rings were observed. It should be noticed that the zero value of the x-axis corresponds to the beginning of each external ring.

of the substrate. We found that a minimum particle concentration ($\Phi_V = 1\%$) was required for the formation of ringlike deposits using the CSSD technique. The width and height of the external ring increased as the concentration increased from $\Phi_V = 1$ to 3%. At $\Phi_V = 5\%$, instead of a wider and higher ring, two concentric ring-like deposits were unexpectedly obtained (see Fig. 5). At $\Phi_V = 7\%$, a wide ring followed by a layer was found and finally, an irregular layer was obtained at $\Phi_V = 10\%$. We observed that for increasing particle concentration ($\Phi_V \geq 3\%$ excluding 5%), the width of the ringlike deposit increased whereas the height reached certain value ($\approx$16.5 μm). Next, the particle deposits grew in the horizontal direction and a varying thickness layer was obtained. The different deposit patterns obtained by varying the nanoparticle volume fraction correlate with the pinning time of each contact line (see Fig. 4). These results were confirmed using larger silica particles, except that with these particles no multiple rings were observed. The occurrence of multiring patterns (Bi et al., 2012) depends on certain conditions, particularly of solute concentration, although a universal mechanism is not clear yet.

3.2 Pinning Time

To study the effect of varying the pinning time with the CSSD technique using nanoparticle suspensions, we selected PMMA suspensions and PMMA substrates. Unlike the PMMA-SiO_2 system examined in Sec. 3.1, the PMMA-PMMA system enabled the plausible effect of wettability contrast to be minimized. We assumed that the receding contact angles of PMMA substrates measured in a previous work (Moraila-Martínez et al., 2012) agreed with the contact angles of the corresponding nanoparticles. This way, the results obtained were mostly dependent on the pinning time and the nanoparticle concentration. We prepared PMMA suspensions at $\Phi_V = 0.1\%$, 1%, and 5% and pH 2. We carried out the different pinning time experiments listed in Table 1. When t_p was reduced from a reference value (140 s) to 30 s, we found that no ringlike deposit was obtained, regardless of nanoparticle concentration. This result is in agreement with those ones obtained with freely evaporating colloidal drops (Shen et al., 2010).

The contact line dynamics of the experiments performed at $\Phi_V = 0.1\%$ is shown in Fig. 6(a). With the PT-1 process, the contact line behaved such as for pure liquids until $r_c = 0.62 r_{\max}$, where a pinning event was observed. Next, the contact angle decreased while the contact line receded until the process finished. Instead of ringlike deposits, a few isolated deposits were formed. With the PT-2 process, an irregular contact line motion was observed during the entire drop receding. Alike the PT-1 process, unresolved ringlike deposits were observed. With the PT-3 process, from the first pinning event, three marked pinning events were formed. The final deposit was a thin ring. With the PT-4 process, the contact line was pinned from the beginning of the process, the contact angle decreased up to $\approx 30^\circ$, and then the contact line receded. During this receding motion, several stick-slip events were observed. The final deposit

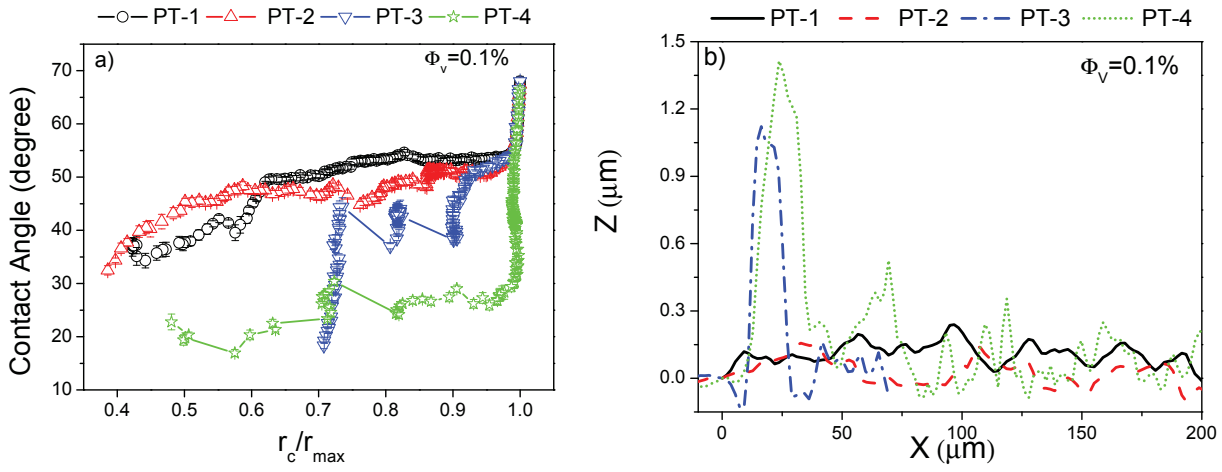

FIG. 6: (**a**) Contact line dynamics and (**b**) profiles of the ringlike deposits formed with PMMA suspensions on PMMA substrates at $\Phi_V = 0.1\%$ and pH 2, at different pinning times (see Table 1).

was also a thin ring. The results obtained show that with a low particle concentration, the deposits appear if the pinning time is accordingly increased. When the pinning time is long enough, a great number of nanoparticles are transported toward the contact line, where they can form a well-defined, ringlike deposit. This way, prolonging the pinning for a given substrate-nanoparticle system seems to be equivalent to increasing the nanoparticle bulk concentration (see Sec. 3.1). The profiles of the deposits obtained with the different pinning time processes are shown in Fig. 6(b). With the PT-1 and PT-2 processes, no ringlike deposit was formed, although a few incomplete deposits were observed. Instead, for the PT-3 and PT-4 processes, thin ringlike deposits were found. As expected, the width and height of the ringlike deposit increased as the pinning time.

The contact line dynamics of the different pinning time experiments at $\Phi_V = 1\%$ is shown in Fig. 7(a). The PT-1, PT-2, and PT-3 processes provided similar contact line dynamics. A first pinning was observed, the contact angle decreased up to the PMMA receding contact angle, and the contact line moved back. During the receding motion of the contact line, a marked stick-slip behavior was observed and a final ringlike deposit was formed. However, with the PT-4 process, the contact line remained pinned while the contact angle decreased up to $\approx 20^\circ$. Next, the contact line receded until the process finished. During the receding motion, stick-slip behavior was also observed and the final deposit was a ring. In Fig. 7(b), the profiles of the ring-like deposits obtained for the different pinning time experiments are shown. Again, the width and height of the ringlike deposit increased with the pinning time. The deposit produced with the PT-1 experiment was the smallest and thinner ring. The deposit profiles obtained with the PT-2 and PT-3 processes were similar in covered area and height, due to the closer pinning times of both processes. The ringlike deposit formed with the PT-4 process was clearly the highest and widest ring. Unlike the case $\Phi_V = 0.1\%$, the four processes produced ringlike deposits at $\Phi_V = 1\%$ and, as expected, they were higher and wider than the deposits obtained at $\Phi_V = 0.1\%$ with the PT-3 and PT-4 processes.

At $\Phi_V = 5\%$ [see Fig. 8(a)], the results show that the contact line remained macroscopically pinned during the entire process, except for the PT-1 process in which, after the first pinning event, the contact line receded for a short time until it was strongly pinned. The contact line jumped from a very low contact angle of $\approx 15^\circ$ and receded till the process finished. The profiles of the ringlike deposits are plotted in Fig. 8(b). With the PT-1, PT-2, and PT-3 processes, the width and height of the ring deposit increased with the pinning time, the profiles obtained with PT-2 and PT-3 being very similar. Instead, with the PT-4 process, the highest and widest ring was formed again, but it was followed by a continuous thick layer. The thickness of this layer (≈ 15 μm) is in agreement with the maximum height of the deposits obtained in Sec. 3.1. This value might depend on the strength of the electrostatic interactions, the substrate receding contact angle, and the particle size. Further work should be addressed to explain this effect.

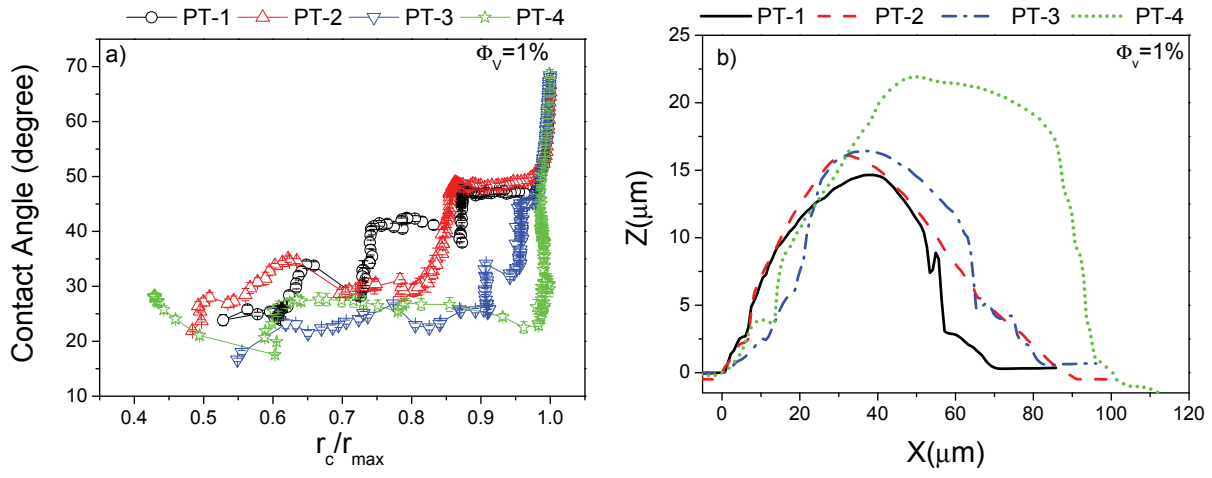

FIG. 7: (**a**) Contact line dynamics and (**b**) profiles of the ringlike deposits formed with PMMA suspensions on PMMA substrates at $\Phi_V = 1\%$ and pH 2, with CSSD experiments at different pinning times (see Table 1).

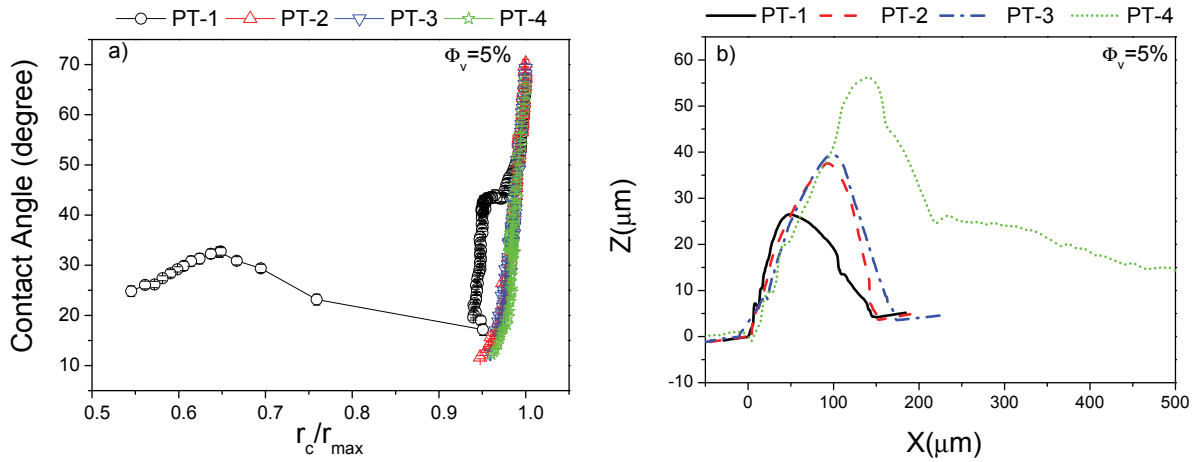

FIG. 8: (**a**) Contact line dynamics and (**b**) profiles of the ringlike deposits formed with PMMA suspensions on PMMA substrates at $\Phi_V = 5\%$ and pH 2, at different pinning times (see Table 1).

We summarize in Fig. 9 all the CSSD experiments performed for the different particle concentrations. To analyze the differences in the morphology of the ringlike deposits, we plot the dimensions of the deposits for each CSSD process (different pinning times). We represent the height and width of the ringlike deposits extracted from the profile analysis. The error bars represent the standard deviation of the results obtained for three profiles of a deposit and averaged over three different deposits. As expected, the highest and widest ring was obtained with the maximum pinning time and highest particle concentration.

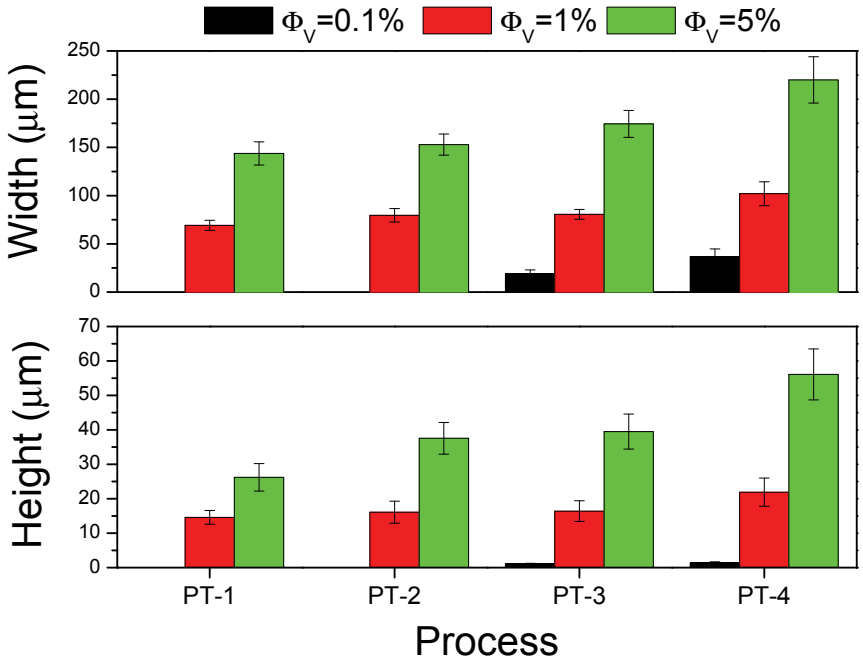

FIG. 9: Characteristic dimensions of the ringlike deposits (height and width) obtained with different pinning times and for different particle concentrations.

To compare the results obtained when the substrate-particle system was varied, we reproduced the four pinning time processes with 90 nm SiO_2 particle suspension (pH 2 and similar diameter ≈100 nm) and varying particle concentration as well (results not shown). Unexpectedly, we found that ring-like deposits formed even when the longest pinning time (PT-4) and higher particle concentration ($\Phi_V = 10\%$) were smaller than those obtained with the PMMA suspensions. Montes Ruiz-Cabello et al. (2013) observed short-range interparticle forces at pH 2 which seem to be particularly important at higher surface potentials. This observation suggests that additional short-range attractions are present, and they could be due to attractive hydrophobic interactions. Hence our results obtained with the PMMA-PMMA system, leading to higher ringlike deposits, can be explained due to attractive hydrophobic interactions between the hydrophobic particles once they are confined near the triple line. To the best of our knowledge, this is the first evidence of the impact of hydrophobic forces on the convective-capillary deposition of nanoparticles.

4. CONCLUSIONS

The most relevant conclusions of this study are summarized as follows:

- Once the electrostatic interactions in the substrate-particle system are minimized, as the nanoparticle concentration increases, the deposit formed from driven receding contact lines using the CSSD technique increases in width and height up to a maximum height. A minimum concentration is required for the formation of ringlike deposits, but above a certain concentration, the ring becomes a particulate film. The role of collective diffusion of colloidal suspensions in drying phenomena should be taken into account, even with weakly charged particles.
- We were able to form ringlike deposits with controlled pinning time using the CSSD technique. Alike nanoparticle concentration, pinning time plays a relevant role for the deposit formation. No nanoparticle deposit is formed if the pinning time is reduced below a critical value, as reported by Shen et al. (2010). However, an increase of pinning time enables the ring formation even at low particle concentration.
- The hydrophobic interparticle interactions may lead to the formation of higher ringlike deposits. Further work should address this.

REFERENCES

Askounis, A., Sefiane, K., Koutsos, V., and Shanahan, M. E., The effect of evaporation kinetics on nanoparticle structuring within contact line deposits of volatile drops, *Colloids Surf.*, vol. **441**, pp. 855–866, 2014.

Bhardwaj, R., Fang, X., Somasundaran, P., and Attinger, D. Self-assembly of colloidal particles from evaporating droplets: Role of DLVO interactions and proposition of a phase diagram, *Langmuir*, vol. **26**, no. 11, pp. 7833–7842, 2010.

Bi, W., Wu, X., and Yeow, E. K. L., Unconventional multiple ring structure formation from evaporation-induced self-assembly of polymers, *Langmuir*, vol. **28**, no. 30, pp. 11056–11063, 2012.

Bodiguel, H., Doumenc, F., and Guerrier, B., Pattern formation during the drying of a colloidal suspension, *Eur. Phys. J. Spec. Top.*, vol. **166**, pp. 29–32, 2009.

Carle, F. and Brutin, D., How surface functional groups influence fracturation in nanofluid droplet dry-outs, *Langmuir*, vol. **29**, no. 32, pp. 9962–9966, 2013.

Deegan, R. D., Bakajin, O., Dupont, T. F., Huber, G., Nagel, S. R., and Witten, T. A., Capillary flow as the cause of ring stains from dried liquid drops, *Nature*, vol. **389**, pp. 827–829, 1997.

Erbil, H. Y., Evaporation of pure liquid sessile and spherical suspended drops: A review, *Adv. Colloid Interface Sci.*, vol. **170**, nos. 1-2, pp. 67–86, 2012.

Kobayashi, M., Juillerat, F., Galletto, P., Bowen, P., and Borkovec, M., Aggregation and charging of colloidal silica particles: Effect of particle size, Langmuir, vol. **21**, no. 13, pp. 5761–5769, 2005.

Lee, D., Kwon, M.-S., Hyun, J.-C., Jun, C.-D., Chung, E., and Yang, S. Protein patterning utilizing region-specific control of wettability by surface modification under atmospheric pressure, *Appl. Phys. Lett.*, vol. **103**, no. 12, pp. 123701–123705, 2013.

Li, Y.-F., Sheng, Y.-J., and Tsao, H.-K., Evaporation stains: Suppressing the coffee-ring effect by contact angle hysteresis, Langmuir, vol. **29**, no. 25, pp. 7802–7811, 2013.

Lopes, M. C. and Bonaccurso, E., Influence of substrate elasticity on particle deposition patterns from evaporating water-silica suspension droplets, *Soft Matter*, vol. **9**, pp. 7942–7950, 2013.

Majumder, M., Rendall, C. S., Eukel, J. A., Wang, J. Y. L., Behabtu, N., Pint, C. L., Liu, T.-Y., Orbaek, A. W., Mirri, F., Nam, J., Barron, A. R., Hauge, R. H., Schmid, H. K., and Pasquali, M., Overcoming the "Coffee-Stain" Effect by Compositional Marangoni-Flow-Assisted Drop-Drying, *J. Phys. Chem. B*, vol. **116**, no. 22, pp. 6536–6542, 2012.

Montes Ruiz-Cabello, F. J., Maroni, P., and Borkovec, M., Direct measurements of forces between different charged colloidal particles and their prediction by the theory of Derjaguin, Landau, Verwey, and Overbeek (DLVO), *J. Chem. Phys.*, vol. **138**, no. 23, p. 234705, 2013.

Moraila-Martínez, C. L., Montes Ruiz-Cabello, F. J., Cabrerizo-Vílchez, M. A., and Rodríguez-Valverde, M. A., The effect of contact line dynamics and drop formation on measured values of receding contact angle at very low capillary numbers, *Colloids Surf., A*, vol. **404**, pp. 63–69, 2012.

Moraila-Martínez, C. L., Cabrerizo-Vílchez, M. A., and Rodríguez-Valverde, M. A., The role of the electrostatic double layer interactions in the formation of nanoparticle ringlike deposits at driven receding contact lines, *Soft Matter*, vol. **9**, pp. 1664–1673, 2013.

Perelaer, J., Smith, P. J., Hendriks, C. E., van den Berg, A. M. J., and Schubert, U. S., The preferential deposition of silica microparticles at the boundary of inkjet printed droplets, *Soft Matter*, vol. **4**, pp. 1072–1078, 2008.

Shen, X., Ho, C.-M., and Wong, T.-S., Minimal size of coffee ring structure, *J. Phys. Chem. B*, vol. **114**, no. 16, pp. 5269–5274, 2010.

Yunker, P. J., Still, T., Lohr, M. A., and Yodh, A. G., Suppression of the coffee-ring effect by shape-dependent capillary interactions, Nature, vol. **476**, no. 7360, pp. 308–311, 2011.